RESEARCH ARTICLE

Synthesis of Silver Nanoparticles by Pulsed Laser Ablation: Structural, Optical, *in vitro* Antibacterial, and Cytotoxicity Properties

Ali M. Ahmed[1,*], Muna B. Mustafa[2], Doaa Hameed Kadhim[3], Mustafa Adnan Zaidan[4], Russul M. Shehab[2]

[1]College of Medicine, Mustansiriyah University, Baghdad 10052, Iraq
[2]Electrical Engineering Technical College, Middle Technical University, Baghdad 10071, Iraq
[3]Department of Physiology, College of Medicine, Mustansiriyah University, Baghdad 10052, Iraq
[4]Medical Technical College, Al-Farahidi University, Baghdad 10069, Iraq

*Corresponding author. Email: ali.majeed@uomustansiriyah.edu.iq

Received date: Apr 19, 2026; Revised date: Jun 9, 2026; Accepted date: Jun 17, 2026

Abstract

BACKGROUND: Silver nanoparticles (AgNPs) are commonly synthesized by chemical methods; however, these methods often involve toxic chemicals that may limit their biomedical applications. In contrast, pulsed laser ablation in liquid (PLAL) is a clean and chemical-free technique capable of producing highly pure AgNPs. Yet, only limited studies have investigated the structural, optical, antibacterial, and cytotoxicity properties of AgNPs synthesized by PLAL. Therefore, this study was conducted to synthesize pure AgNPs using pulsed laser ablation and evaluate their biomedical activity against bacterial strains and MCF-7 cells.

METHODS: The synthesis of AgNPs was done by PLAL technique, and the characterization of nanoparticles were further determined using transmission electron microscopy (TEM), X-ray diffraction (XRD), and Ultraviolet-Visible (UV–Vis) spectroscopy. Antibacterial activity of AgNPs was tested with agar well diffusion method and the cytotoxicity effect was evaluated with MTT assay against the MCF-7 cells.

RESULTS: TEM analysis showed semi-spherical AgNPs with an average particle size of 31 nm. XRD analysis showed that the structure was crystalline face-centered cubic with an average crystallite size of 16.8 nm. Peak value of the SPR was recorded at 405 nm and the optical band gap was 2.28 eV. Concentration dependent antibacterial activity was observed for the AgNPs and inhibition zones of 17 mm against *Streptococcus mutans* and 18 mm against *Lactobacillus* spp. at highest concentration. Moreover, concentration-dependent cytotoxicity against MCF-7 cells was observed, reaching a maximum inhibition of about 69% at 1000 µg/mL and IC_{50} of about 90 µg/mL.

CONCLUSION: The synthesized AgNPs showed favorable structural and optical characteristics, along with antibacterial and cytotoxic activities. Both effects were concentration-dependent, indicating their potential for further biomedical applications.

KEYWORDS: silver nanoparticles, laser ablation, antibacterial activity, MCF-7, cytotoxicity

Indones Biomed J. 2026; 2026; 18(3): 213-22

Introduction

Nanoparticles are defined as particles sized within the range of 1 to 100 nm, and are an important area of nanoscience and nanotechnology.(1,2) The unique physical, chemical and biological properties of nanoparticles are attributed to their small size and high surface area to volume ratio compared with bulk materials.(3,4) These unique properties have allowed them to be used in a range of applications such as environmental decontamination, electronics, and biomedical engineering.(5) Silver nanoparticles (AgNPs) have gained

special attention because of their optical, antibacterial, and cytotoxic properties, which are strongly influenced by particle size, morphology, and surface properties.

AgNPs are one of the forms of nanoparticles that have received significant attention because of their excellent antimicrobial, optical, and catalytic qualities.(6) Particle size, morphology, and concentration are factors that have a strong effect on the biological activity of AgNPs.(7) Nanoparticle fabrication methods have been variedly made such as, physical, chemical and biological.(8) Nonetheless, green (environmentally friendly) methods of synthesis have received more and more attention as they are safe, cost-effective, and do not produce toxic waste.(9)

The synthesis of the AgNPs has been reported by various conventional chemical methods, but generally the reducing agents and stabilizing compounds used in the synthesis process are small molecules that can remain attached to the surface of the nanoparticles.(10) These chemicals residues may require further purification and may affect the biological activity of the manufactured nanoparticles. Hence, alternative methods like pulsed laser ablation in liquid (PLAL) have attracted significant interest as they enable the production of high purity nanoparticles without the need for chemical reductants or stabilizers.(11) PLAL is also regarded as one of the most promising physical techniques of nanoparticle syntheses that are environmentally friendly.(12) Such a method has a number of advantages such as purity is high, the particle size can be accurately determined, and chemical contaminants are removed. Thus, laser ablation produces AgNPs that can be useful in the development of antimicrobial and cytotoxic applications.(13)

AgNPs have been widely researched on its ability to exhibit antibacterial effects against a large group of pathogenic microorganisms.(14) Their action is principally due to their capacity to disrupt cell membranes, form reactive oxygen species (ROS), and disrupt cellular components including DNA and proteins.(15) AgNPs have also shown great potential in cancer research besides their antimicrobial properties.(16) *Streptococcus mutans* and *Lactobacillus* spp. are known as representative oral pathogenic bacteria was based on their proven involvement in the development of dental plaque and progression of dental caries. In addition, the microorganisms are commonly used in antibacterial studies with AgNPs, which makes it possible to make more meaningful comparisons with previous reports of studies.

Cancer is one of the major causes of death in the world, and its absence of control over cell proliferation, as well as the capacity to invade the adjacent tissue, characterize it.(17) The recent research works have examined the cytotoxic properties of AgNPs with cancerous cells and the findings showed that their action greatly relies on the size of particles, concentration and the method of synthesis.(18) The reduced size of nanoparticles is more likely to result in high cellular uptake and biological activity. Generation of ROS, causing oxidative stress, dysfunction of the mitochondrion, and DNA damage are the major cytotoxic effects of AgNPs.(19)

In the present work, the synthesis of AgNPs was carried out by the clean and chemical-free technique of PLAL. The synthesized AgNPs were characterized using structural and optical methods and their antibacterial and cytotoxic activities were examined. The antibacterial activity was evaluated against the two Gram-positive bacteria, *S. mutans* and *Lactobacillus* spp. which are commonly used in antimicrobial studies. The synthesized AgNPs also exhibited cytotoxic activity against the breast cancer cells MCF-7. The objective of the study was to assess the correlation between the physicochemical properties of the AgNPs and the biological activity observed.

Methods

Preparation of AgNPs

AgNPs were prepared by the PLAL technique.(20) The high-purity silver target plate (99.99%) was cleaned with acetone and ethanol, rinsed with deionized water, and then positioned at the bottom of a glass vessel with 3 mL of deionized water. The liquid level was maintained 5 mm above the target level. The wavelength of the Nd:YAG pulsed laser used for the ablation was 1064 nm.(21) In the laser ablation process, the silver target was placed on a rotary table and rotated throughout the process to prevent repeated irradiation of the same area on the target, and to promote more uniform production of the nanoparticles.

The laser parameters were a pulse repetition rate of 1 Hz, a pulse energy of 650 mJ, a pulse duration of 9 ns and a total of 350 laser pulses. During the ablation process, the laser beam was incident on the silver target surface at a distance of 10 cm. The synthesis was performed in the normal laboratory atmosphere. This colloidal AgNP solution was used as the stock solution for further antibacterial and cytotoxicity assays.(22)

During the same experiment, the ablation process was carried out under ambient laboratory conditions with the target held at rest. The obtained colloidal solution exhibited

a yellowish color, which may indicate the formation of AgNPs. The formation of AgNPs was further confirmed by transmission electron microscopy (TEM), X-ray diffraction (XRD), and Ultraviolet-Visible (UV–Vis) analyses. The resultant colloid was further analyzed in terms of its structural, optical, antibacterial, and cytotoxic properties.

Characterization of AgNPs

TEM (ZEISS LEO 912, 100 k V; Zeiss, Oberkochen, Germany) was used to determine the morphology and particle size of the synthesized AgNPs. The AgNP powder after sedimentation was subjected to TEM analysis. ImageJ software (National Institutes of Health, Bethesda, MD, USA) was used to measure the average size of the particles and size distribution.

Meanwhile, the XRD was used to determine the crystalline structure using an XRD-6000 diffractometer (Shimadzu, Kyoto, Japan) with CuKα radiation in the scan range of 20–80°. X'Pert HighScore Plus software (Malvern Panalytical, Malvern, UK) was used to analyze the diffraction patterns and compare them to standard reference data. The Scherrer equation was applied in determining the crystallite size of the AgNPs: $D = (0.9\lambda)/(\beta \cos \theta$ (23), where D was the crystallite size, λ was the wavelength of the CuKα radiation (1.5406 Å) and β was the half width at half maximum (FWHM) of the diffraction peak in radians, and θ was the Bragg diffraction angle. All the values of FWHM obtained from the XRD peaks were converted into radians prior to calculating. Besides the determination of crystallite size, the dislocation density (δ) and microstrain (ε) were determined as follow : $\delta = 1/D2$; and $\varepsilon = \beta/4 \tan \theta$ (24), where β was the FWHM of the diffraction peak and θ was the Bragg diffraction angle.

An optical study of the nanoparticles was performed with the help of a double-beam UV-visible (UV-Vis) spectrophotometer (Shimadzu Model 1200; Shimadzu) at a wavelength ranging between 200 and 1000 nm, the blank solution used was deionized water and the colloidal AgNP solution was analysed without dilution.

Antibacterial Activity

Agar well diffusion method was used to evaluate the antibacterial activity of the AgNPs synthesized against some bacterial strains including *S. mutans* and *Lactobacillus* spp. (25) Aseptic preparation A sterile petri plates were prepared in sterile Mueller-Hinton agar medium and estimated 20 mL of the molten medium was added and permitted to solidify. (26) Fresh bacterial cultures the bacterial inoculum density was adjusted to 0.5 McFarland standard were taken out of stock cultures and evenly spread all over the surface of the solidified agar plates to facilitate even growth of the bacteria. Circular wells of 6 mm diameter were then carefully drawn in the agar using sterile pipette tips after inoculation. Aliquots of the made AgNP colloidal suspension with various concentrations were subsequently pipette into the wells, the description of the antibacterial assay was revised and clarified. The actual volumes and concentrations for dispensing were not obtained from the original experiments.(27) The ready plates were then placed in 37°C and left to incubate after 72 h to enable bacterial growth and diffusion of the nanoparticles through the agar plate. After incubation the definite circle of clearances occurred around the wells and these were measured in millimeters. The diameter of the inhibition zones was determined and it was applied to determine the antibacterial activity of synthesized AgNPs against the microorganisms that were tested.(28) However, the agar well diffusion method is based on diffusion of nanoparticles into the agar and can only be used as a preliminary method to assess antibacterial activity.

MTT Assay

The MTT assay on cytotoxicity of the AgNPs synthesized was tested against MCF-7 cell line of breast cancer, to calculate the percentage of cell cytotoxicity induced by AgNPs, MTT assay was used. Cells were grown in 96-well plates at a 1×10^5 cell density and incubated over 72 hours at 37°C in a humid environment with 5% CO_2 under humidified incubation conditions to get cells attached to the wells and stabilized. The incubation phase was followed by removal of the culture media and washing of cells twice in phosphate buffered saline (PBS) to remove any leftover media. Each well was then added with fresh RPMI culture medium containing 10 percent fetal bovine serum (FBS). These cells were then subjected to the varying concentrations of AgNPs (0.1, 1, 10, 100 and 1000 µg/mL) and incubated over 72 h according to references.(28,29) The control group was untreated cells and each concentration was conducted in three wells.

After the exposure time, 10 µL of MTT solution (5 mg/mL in PBS) was placed in each well and the plates were subsequently incubated in 4 h to enable the development of formazan crystals. After that, the culture medium was removed carefully followed by 100 µL of dimethyl sulfoxide (DMSO) that dissolved the crystal that formed. The plates were carefully shaken in order to make sure complete dissolution. The MCF-7 breast cancer cells AgNPs cytotoxicity was then examined using microplate reader

(STAT FAX 2100; BioTek, Winooski, VT, USA) to measure the absorbance at 545 nm. The absorbance wavelength used in the study was chosen based on the microplate reader's specifications. The proportion of cell toxicity was computed using the values of optical density (OD50), along with a half-maximal inhibitory concentration (IC_{50}). The IC_{50} value was determined by plotting the dose–response curve for cell cytotoxicity and fitting the curve to a standard dose–response model. The percentage of cytotoxicity was calculated using the following equation (29):

$$\text{Toxicity (\%)} = \left(1 - \frac{\text{mean OD of sample}}{\text{mean OD of control}}\right) \times 100$$

Results

Crystalline Structure and Phase Composition of AgNPs

XRD was used to determine the crystalline structure and to confirm the purity of the synthesized AgNPs. The diffraction pattern in the 2θ range of 20-80° was well defined with a number of peaks that are associated with crystalline metallic silver. In the diffractogram, there were four unique diffraction peaks at 38.35, 44.20, 64.70 and 77.30 degrees that could be indexed to the (111), (200), (220) and (311) planes of face centered cubic (fcc) silver (Figure 1). The reflection at the highest (111) position with the highest intensity was at 38.35 and that forms a reflection, giving evidence that this was the desired plane of growth of the synthesized nanoparticles. In addition, the steepness of the diffraction peaks indicates that the prepared nanoparticles were very crystalline.

The sizes of the crystallites of various planes of diffraction were calculated to be between 93.40 and 114.25 nm with a mean value of about 105 nm (Table 1). The values of dislocation density were between 7.66 10 -5 to 1.146 10-5 nm-2 and the values of microstrains were between 3.01 × 10^{-4} to 3.68 × 10^{-4}.

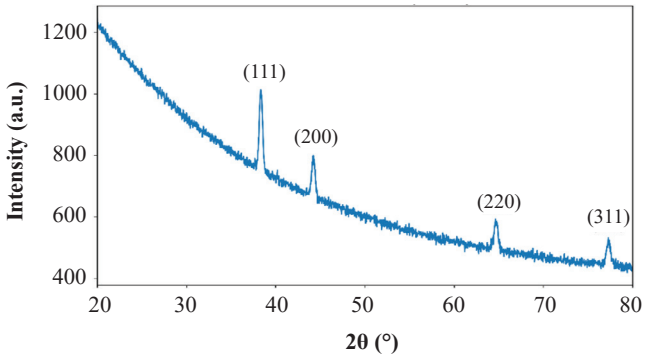

Figure 1. XRD pattern of AgNPs.

Morphology and Size Distribution of AgNPs

The morphology and size distribution of the synthesized AgNPs were studied using TEM. Figure 2 showed the representative TEM micrographs at various magnifications (300 nm and 40 nm scale bars). The TEM images have certainly verified successful formation of silver nanoparticles with major nearly spherical morphology. The nanoparticles seemed to be fairly distributed over the substrate, yet some slight extent of clustering of the particles could be seen.

In order to measure the size of the distribution of the particle size quantitatively, measurements have been made using ImageJ software in the basis of a number of TEM images (Figure 3). The histogram reveals that most of the nanoparticles are in the size range of about 18-45 nm and the average particle size is about 31 nm. The size distribution was rather homogeneous. Most nanoparticles were found to be within the range of 30–35 nm which indicates a narrow particle size distribution. The average particle size was estimated to be 31±3.5 nm.

Optical Properties of AgNPs

UV-Vis spectroscopy was used to determine the optical characteristics of the AgNPs that were synthesized. Figure 4 showed the UV-Vis absorption spectrum of the AgNPs prepared in the wavelength span of 250-800 nm. It was observed that a wide and strong absorption band was located at around 405 nm.

The optical band gap of the AgNPs synthesized was estimated. The Tauc plot was presented in Figure 5. The optical transition behavior of the synthesized AgNPs was estimated by the Tauc plot analysis under assumption of direct electronic transition model. The optical band gap energy of the AgNPs was calculated to be approximately 2.28 eV.

Antibacterial Activity of AgNPs

The agar well diffusion test was used to determine the antibacterial activity of the synthesized AgNPs on two bacterial strains, namely *S. mutans* and *Lactobacillus* spp. The results of the inhibition zones at the various concentrations are tabulated in Table 2 and depicted in Figure 6, it was shown that the negative control had no zone of inhibition.

The findings indicate that AgNPs that have been synthesized have antibacterial activity against the two strains tested. The size of the inhibition zones increased with increasing nanoparticle concentration. The most effective antibacterial activity was exhibited at the highest AgNP concentration against both of the bacterial isolates.

Table 1. XRD parameters of AgNPs.

2θ (°)	d-spacing (Å)	FWHM (°)	(hkl)	Crystallite Size (nm)	Dislocation Density ($\times10^{-3}$ nm^{-2})	Strain ($\times10^{3}$)
38.350	2.347	0.072	-111	114.25	0.0766	0.301
44.200	2.048	0.091	-200	93.40	0.1146	0.368
64.700	1.438	0.092	-220	102.85	0.0945	0.336
77.300	1.228	0.094	-311	110.10	0.0824	0.309

The synthesized AgNPs exhibited concentration dependent antibacterial activity against the bacteria, *S. mutans* and *Lactobacillus* spp. The highest concentration of AgNPs resulted in the largest inhibition zone diameters of *S. mutans* and *Lactobacillus* spp. at 17±0.8 mm and 18±1.1 mm, respectively.

Cytotoxic Effects of AgNPs on MCF-7 Cells

The cytotoxic effect of the synthesized AgNPs against MCF-7 breast cancer cells was evaluated using the MTT assay. Figure 7 demonstrated that the cytotoxicity of AgNPs was analyzed with the concentration of 0.1–1000 µg/mL. The results have shown a concentration dependent anti-proliferative effect with the viability of the MCF-7 cells decreasing as the AgNP concentration increased.

The findings have given a concentration-dependent cytotoxic effect whereby cell inhibition increased with increasing AgNP concentration. The maximum concentration produced about approximately 69% cytotoxicity, the highest tested concentration (1000µg/mL) showed the maximum inhibition. AgNPs IC_{50} value was determined to be around 90 µg/mL, The IC_{50} value was determined by non-linear regression analysis.

Discussion

These results agree well with the conventional diffraction data of metallic silver (No. 00-004-0783), which indicates that the synthesis of the metallic AgNPs with no detectable secondary phases or crystalline oxide impurities in the standard diffraction technique is successful.(30) Silver nanostructures are usually reported to be dominated by the (111) plane as it has a relatively low surface energy.(31)

Such findings reveal that the nanoscale crystal domains are developed in the process of laser ablation. These are comparatively low values which means that the AgNPs synthesized have an intermediate degree of lattice distortion and structural defects.(32) The calculated dislocation density and microstrain values suggest that there is an intermediate amount of lattice distortion in the synthesized silver nanostructure. Microstrain and dislocations may be explained by the fact that the nucleation and solidification of the product during the liquid ablation by pulsed laser takes place rapidly.(33) Using high-energy laser pulses may cause local melting and atmospheric discharge at the metal surface, and the liquid media will suppress the process which may

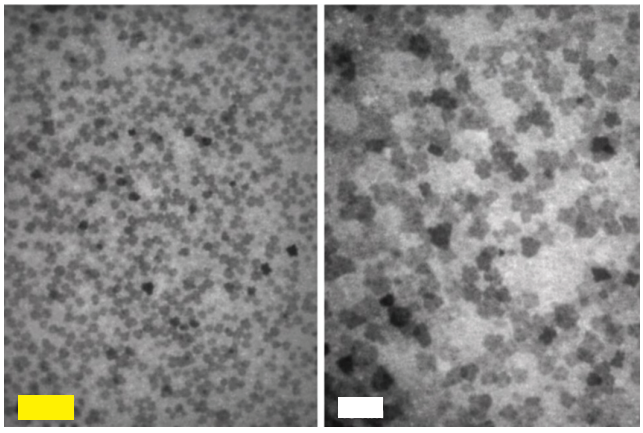

Figure 2. TEM images and corresponding particle size distribution histogram of synthesized AgNPs. Yellow bar: 300 nm; White bar: 40 nm.

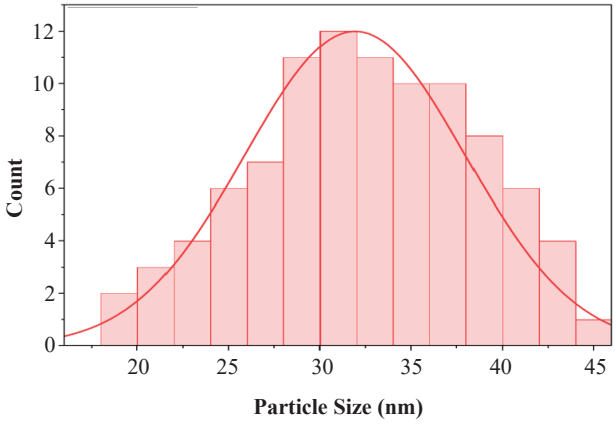

Figure 3. The quantitative distribution of the particle size based on the TEM images. The calculated average particle size was 31 nm.

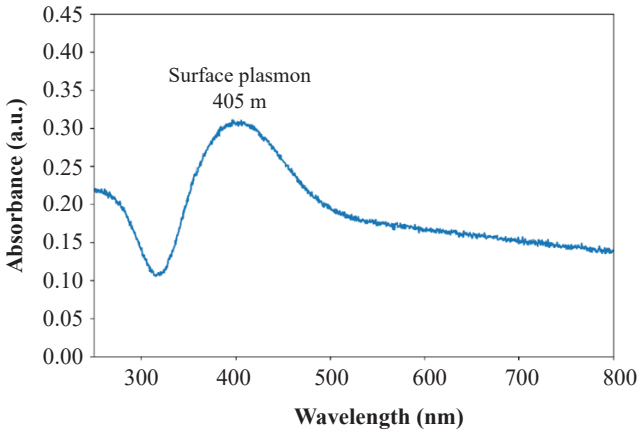

Figure 4. UV–Vis absorption spectrum of AgNPs.

contribute to the creation of slight distortions in the lattice of the growing nanoparticles. In general, the outcomes of the XRD indicate that the prepared AgNPs have a highly crystalline face-centered cubic structure.(34) The difference of the estimated crystallite size, derived from XRD (~105 nm), and the average particle size obtained from TEM (~31 nm) can be explained by the fact that the XRD measures coherent diffraction domains while the TEM image uses the actual size of the particles.

The nanoparticles seem to be homogeneously dispersed over the substrate, yet some slight extent of clustering of the particles could be seen. Interactions between particles in the nucleation and growth processes usually result in such clustering being commonly reported in nanoparticles synthesized through pulsed laser ablation in liquids.(35) The size distribution is fairly consistent, which implies that the morphology of the synthesized nanoparticles is relatively uniform and the dispersion is moderate. It is also possible to explain the formation of nanoparticles in this size regime by the controlled parameter of laser ablation, which also affects nucleation dynamics and growth of particles during the synthesis. The high surface to volume ratio of the AgNPs is due to their nanoscale size and is an important parameter that increases the physicochemical and biological characteristics of the nanoparticles.(36) The physicochemical properties can be a factor involved in the antibacterial and cytotoxic activities that were observed for the synthesized AgNPs.

The optical response of metallic nanoparticles is strongly dependent on the size, morphology and concentration of the particles, and for this reason, UV–Vis spectroscopy is a common technique to determine the optical response of these particles.(37) The presence of the plasmonic peak indicates that the AgNPs were successfully created in the colloidal solution. The large surface plasmon resonance (SPR) band suggests that there is a range of particle sizes, as the TEM images suggest the presence of nanoparticles in the nanometer size range. This feature may be attributed to light scattering process and electronic excitation process within the nanoparticle system. In summary, the obtained spectrum has typical optical properties of silver nanoparticles, confirming their plasmonic properties, which are strongly correlated with the size and surface-to-volume ratio of nanoparticles.

The gap value that was observed may be explained by the electronic transitions of the conduction electrons of the silver nanoparticles.(38) The quantum confinement effect and the large surface-to-volume ratio of nanoparticles may be the reason behind the slight variation of optical transition behavior. At the nanoscale, spatial confinement of charge carriers may influence the electronic structure of materials which causes the change in optical and electronic properties. The optical response observed is in agreement with the observations in the XRD and TEM analysis, which show nanoscale dimensions.

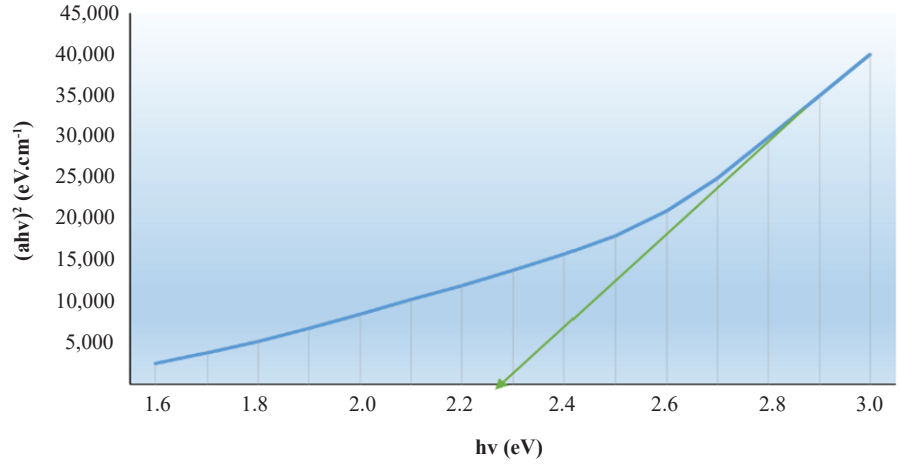

Figure 5. Estimation of the optical band gap of AgNPs using the Tauc plot.

Table 2. AgNPs inhibition zone (mm) of selected bacterial strains in various concentrations.

Bacteria	Control (n)	Concentrations of Ag NPs			
		12.5%	25%	50%	100%
Streptococcus mutans	6	7	8.5	10.5	17
Lactobacillus spp.	6	7.5	9.5	12	18

The increased antibacterial effect of AgNPs is likely to be explained by a number of mechanisms. AgNPs are in the form of nanoparticles, and this fact implies that their surface to volume ratio is high and due to this reason, more surfaces are exposed to interact with bacterial cell membranes.(39) The nanoparticles are capable of binding to bacterial cell wall via electrostatic interaction which may cause perturbation of membrane permeability and structural integrity. The antibacterial activity shown in the present study could be attributed to the nanoscale dimensions and high surface area of AgNPs that could increase interactions with bacterial cell surfaces. The mechanisms that have been reported in previous studies are possible such as silver ion release and oxidative stress generation, a direct investigation of which was not done in the present work.

The cytotoxicity, which is observed, may be associated by the following properties of AgNPs: high surface-to-volume ratio and increased cellular interaction due to the nanoscale.(40) These properties may support cells and their interactions of nanoparticles into cancer cells by means of endocytosis and membrane penetration. After internalization, AgNPs have been reported to interact such as mitochondria, DNA, and cytoplasmic proteins, may influence normal cellular functions. One of the important processes is the production of ROS, which may contribute to oxidative stress in the cells. All in all, these results indicate that the synthesized AgNPs have a concentration-dependent cytotoxic activity impact on MCF-7 cells. The results of this study suggest that these compounds have some preliminary *in vitro* cytotoxic activity but the molecular mechanisms were not experimentally explored in the present study.

There are certain limitations of the current study which should be taken into account. The biological activities were assessed in the *in vitro* conditions and this may not be entirely representative of the *in vivo* behavior. Moreover, a limited number of bacterial strains was studied, as well as a single cancer cell line (MCF-7). Moreover, the long-term stability and a detailed toxicity profile of the produced AgNPs were not thoroughly studied. In addition, in the present study zeta potential analysis was not conducted and hence, the colloidal stability of the synthesized AgNPs in aqueous medium needs to be investigated further. Previous studies have shown that the laser-ablated AgNPs in the aqueous medium might have a temporary colloidal stability because of the electrostatic surface charging as a result of the PLAL process; however, there is still a need for further study into the stability behavior for long-term storage.

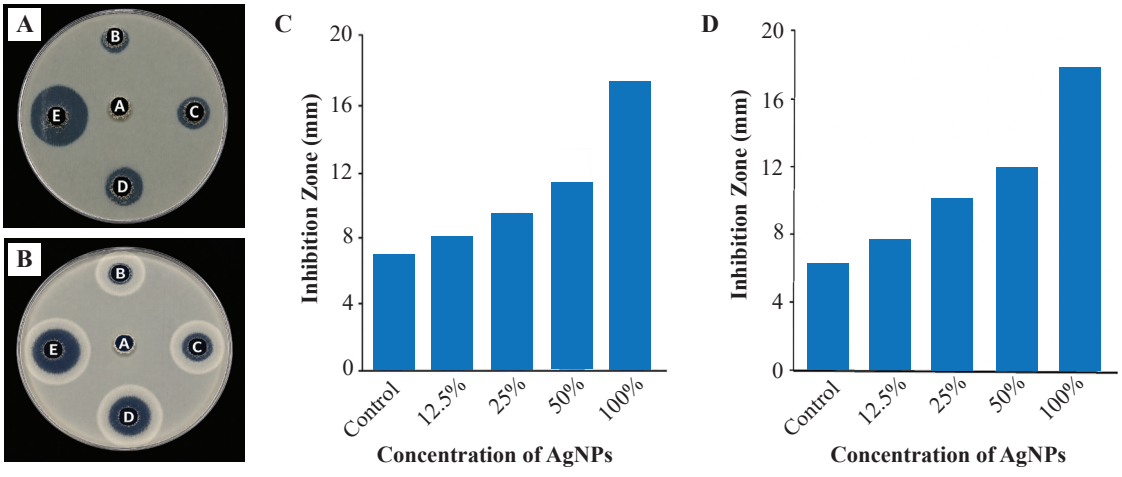

Figure 6. Representation of inhibition zones and inhibition zone diameters of AgNPs towards *S. mutans* and *Lactobacillus* spp. A: inhibition plate of *S. mutants*; B: inhibition plate of *Lactobacillus* spp; C: quantification of the AgNP inhibition zone towards *S. mutants*; D: quantification of the AgNP inhibition zone towards *Lactobacillus* spp.

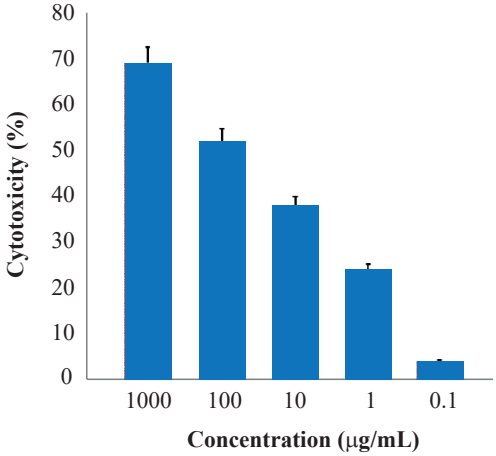

Figure 7. AgNPs cytotoxicity on MCF-7 cells under varying concentrations (0.1-1000 µg/mL) identified using the MTT assay.

It is suggested that future research be done on the *in vivo* biological impact of these nanoparticles with regards to their pharmacokinetics and biocompatibility. In addition, further research is needed on non-cancerous cell lines to investigate selectivity and biocompatibility of the synthesized AgNPs. It would be beneficial to increase the amount of microbial strains and cancer cell lines to allow a better understanding of their therapeutic potential. Further studies with detection of ROS (*e.g.*, by staining with 2',7'-dichlorodihydrofluorescein diacetate (DCFH-DA)), Ag^+ release assays and molecular pathway studies are required to gain insight into the underlying biological mechanisms of the synthesized nanoparticles. In addition, additional refinement of the synthesis parameters can be used to regulate the size of the particles and to increase their functional properties.

Conclusion

The AgNPs were successfully synthesized by PLAL and found to have a primarily semi-spherical shape and an average diameter of 31 nm, respectively. The structural and optical characterization confirmed the crystalline nature of the nanoparticles, the surface plasmon resonance peak was at 405 nm and the optical band gap was about 2.28 eV. The synthesized nanoparticles exhibited concentration-dependent antibacterial property against the growth of *S. mutans* and *Lactobacillus* spp. and also showed concentration-dependent cytotoxicity against MCF-7 cells with an IC_{50} value of around 90 µg/mL. The results suggest that the synthesized silver nanoparticles using PLAL method are applicable in biomedical applications.

Acknowledgments

The authors would like to acknowledge the support provided by their respective institutions for facilitating this research.

Authors Contribution

AM, MA, and RM were involved in the conception and design of the study. AM, MB, DH, MA, and RM participated in data acquisition. AM and MB performed the data analysis. AM, MA, and RM contributed to the interpretation of the results. AM and RM prepared the manuscript, while AM, DH, and MA contributed to figure and table design. All authors critically revised the manuscript and approved the final version for publication.

Ethical Statement

Ethical approval was not required for this study as it did not involve human or animal subjects.

Conflict of Interest

The authors state that they have no conflict of interests as far as publication of the paper is concerned.

References

1. Khan Y, Sadia H, Shah SZA, Khan MN, Shah AA, Ullah N, *et al*. Classification, synthetic, and characterization approaches to nanoparticles, and their applications in various fields of nanotechnology: A review. Catalysts. 2022; 12(11): 1386. doi: 10.3390/catal12111386.
2. Zakinyan A, Ahmed AM, Kononenko D. Local field and deformation of droplets in emulsions. J Mol Liq. 2025; 427: 127406. doi: 10.1016/j.molliq.2025.127406.
3. Joudeh N, Linke D. Nanoparticle classification, physicochemical properties, characterization, and applications: A comprehensive review for biologists. J Nanobiotechnology. 2022; 20(1): 262. doi: 10.1186/s12951-022-01477-8.
4. Kusuma BWA, Dwiningsih SR, As'adi A, Wahyuningsih SPA. Liposome-based nanoparticles encapsulating vitamin D3 attenuate IL-6 and TNF-α in a menopausal mouse model. Indones Biomed J. 2026; 17(5): 484-92.
5. Al-Maathadi A, Karawya F, Al-Dalaen S, Aljabali A, Satari A. Alpha lipoic acid (ALA) alleviates hepatocytes toxicity of titanium dioxide nanoparticles in rats. Indones Biomed J. 2023; 15(3): 231-9.
6. Sati A, Ranade TN, Mali SN, Yasin HKA, Pratap A. Silver nanoparticles (AgNPs): Comprehensive insights into bio/synthesis, key influencing factors, multifaceted applications, and toxicity—an

update. ACS Omega. 2025; 10(8): 7549-82.
7. Menichetti A, Mavridi-Printezi A, Mordini D, Montalti M. Effect of size, shape and surface functionalization on the antibacterial activity of silver nanoparticles. J Funct Biomater. 2023; 14(5): 244. doi: 10.3390/jfb14050244.
8. Ahmed AM, Shehab RM, Khalid GA, Zaidan MA. Manufacturing of zinc oxide nanoparticles for medical applications. Int J Heat Technol. 2025; 43(4): 1567-72.
9. Husham KAF, Khdier HM, Saadoon NM, Ahmed AM. Preparation of CuO/PVA nanocomposite thin films for gamma ray attenuation via PLA method. J Nanostruct. 2024; 14(3): 712-22.
10. Nguyen NPU, Dang NT, Doan L, Nguyen TTH. Synthesis of silver nanoparticles: From conventional to 'modern' methods—A review. Processes. 2023; 11(9): 2617. doi: 10.3390/pr11092617.
11. Fazio E, Gökce B, De Giacomo A, Meneghetti M, Compagnini G, Tommasini M, *et al.* Nanoparticles engineering by pulsed laser ablation in liquids: Concepts and applications. Nanomaterials. 2020; 10(11): 2317. doi: 10.3390/nano10112317.
12. Ahmed AM, Shehab RM, Hammed MAN, Khalid GA, Jaber GS, Zaidan MA. Optimization of copper oxide nanoparticles production by pulsed laser ablation: a study on energy density effects. Ann Chim Sci Mater. 2025; 49(2): 157-62.
13. Khairani IY, Mínguez-Vega G, Doñate-Buendía C, Gökce B. Green nanoparticle synthesis at scale: A perspective on overcoming the limits of pulsed laser ablation in liquids for high-throughput production. Phys Chem Chem Phys. 2023; 25(29): 19380-408.
14. Ahmed AM, Fadhil GA, Rahmah MI. Innovative use of commercial wipes as a template for the synthesis of ZnO and CuO nanoparticles via combustion method for antibacterial applications. Appl Nanosci. 2026; 16(1): 10. doi: 10.1007/s13204-025-03142-6.
15. Ali HM, Karam K, Khan T, Wahab S, Ullah S, Sadiq M. Reactive oxygen species induced oxidative damage to DNA, lipids, and proteins of antibiotic-resistant bacteria by plant-based silver nanoparticles. 3 Biotech. 2023; 13(12): 414. doi: 10.1007/s13205-023-03835-1.
16. Mohamed AF, Nasr M, Amer ME, Abuamara TMM, Abd-Elhay WM, Kaabo HF, et al. Anticancer and antibacterial potentials induced post short-term exposure to electromagnetic field and silver nanoparticles: in vitro study. Infect Agents Cancer. 2022; 17(1): 4. doi: 10.1186/s13027-022-00416-4.
17. Neamah AS, Wadan AHS, Lafta FM, Elakwa DES. The potential role of targeting the leptin receptor as a treatment for breast cancer in the context of hyperleptinemia: a literature review. Naunyn Schmiedebergs Arch Pharmacol. 2025; 398(4): 3451-66.
18. Sati A, Mali SN, Ranade TN, Yadav S, Pratap A. Silver nanoparticles (AgNPs) as a double-edged sword: synthesis, toxicity mechanisms and anticancer potentials. Biol Trace Elem Res. 2026; 204(1): 401-52.
19. Okur EE, Akdaşçi E, Eker F, Bechelany M, Karav S. Silver nanoparticles as anticancer agents: Mechanisms, current studies, and limitations. Pharmaceuticals. 2026; 19(2): 241. doi: 10.3390/ph19020241.
20. Rahmah MI, Ahmed AM, Rashid TM, Qasim AJ. Preparation of silver nanoparticles using laser ablation for in vitro treatment of MCF-7 cancer cells with antibacterial activity. Plasmonics. 2024; 19(4): 2097-105.
21. Ahmed AM, Halim MM, Ahmed NM, Rashid M, Taha BA. Advances in pulsed laser ablation in liquid for silver and copper synthesis: from plasma generation to nanoparticle formation. Physica Status Solidi (a). 2025; 222 (18): 2500382. doi: 10.1002/pssa.202500382.
22. Cîrloiu Boboc GS, Segneanu AE, Bejenaru LE, Văruț MC, Bălăşoiu RM, Călina D, *et al.* Sprayable hybrid gel with cannabidiol, hyaluronic acid, and colloidal silver: A multifunctional approach for skin lesion therapy. Pharmaceutics. 2025; 17(9): 1189. doi: 10.3390/pharmaceutics17091189.
23. Mustapha S, Ndamitso M, Abdulkareem AS, Oladejo JT. Comparative study of crystallite size using Williamson-Hall and Debye-Scherrer plots for ZnO nanoparticles. Adv Nat Sci Nanosci Nanotechnol. 2019; 10(4): 045013. doi: 10.1088/2043-6254/ab52f7.
24. John KI, Adenle AA, Adeleye AT, Onyia IP, Amune-Matthews C, Omorogie MO. Unravelling the effect of crystal dislocation density and microstrain of titanium dioxide nanoparticles on tetracycline removal performance. 2021; 776: 138725. doi: 10.1016/j.cplett.2021.138725.
25. Ghabban H, Alnomasy SF, Almohammed H, Al Idriss OM, Rabea S, Eltahir Y. Antibacterial, cytotoxic, and cellular mechanisms of green synthesized silver nanoparticles against some cariogenic bacteria (Streptococcus mutans and Actinomyces viscosus). J Nanomater. 2022; 2022 (1): 9721736. doi: 10.1155/2022/9721736.
26. Shah BA, Zaman SU, Zeb A, Ullah N, Shah KU. Topical system of Chitosan based hydrogel fabricated with fusidic acid loaded SLNs: A new approach against MRSA related wound infections. J Drug Deliv Sci Technol.2025; 104: 106488. doi: 10.1016/j.jddst.2024.106488.
27. Al-Momani H, Almasri M, Al Balawi DA, Hamed S, Albiss BA, Aldabaibeh N, *et al.* The efficacy of biosynthesized silver nanoparticles against Pseudomonas aeruginosa isolates from cystic fibrosis patients. Sci Rep. 2023; 13: 8876. doi: 10.1038/s41598-023-35919-6.
28. Asif M, Yasmin R, Asif R, Ambreen A, Mustafa M, Umbreen S. Green synthesis of silver nanoparticles (AgNPs), structural characterization, and antibacterial potential. Dose Response. 2022; 20(2): 15593258221088709. doi: 10.1177/15593258221088709.
29. Ebadi M, Zolfaghari MR, Aghaei SS, Zargar M, Shafiei M, Shahbani Zahiri H, *et al.* Bio-inspired synthesis of ZnO nanoparticles using cyanobacterium Nostoc sp. RSC Adv. 2019; 9: 23508-25.
30. Alam MA, Bishwas RK, Mostofa S, Ahmed S, Zannat F, Jahan SA. Study of sol-gel derived silver nanoparticle (AgNPs): X-ray computed crystal growth mechanism and thermal analysis. S Afr J Chem Eng. 2026; 56: 100839. doi: 10.1016/j.sajce.2026.100839.
31. Yang C, Gao C, Zhou W, Gu H, Pan M, Li H, *et al.* Controlling silver deposition morphology on aluminum surfaces: Surfactant modify anisotropy of aluminum surface energy. Surf Interfaces. 2024; (49): 104420. doi: 10.1016/j.surfin.2024.104420.
32. Lasmi F, Hamitouche H, Laribi-Habchi H, Benguerba Y, Chafai N. Silver nanoparticles (AgNPs), methods of synthesis, characterization, and their application: A review. Plasmonics. 2025; 20(11): 9455-88.
33. Korede V, Nagalingam N, Penha FM, van der Linden N, Padding JT, Hartkamp R, et al. A review of laser-induced crystallization from solution. Cryst Growth Des. 2023; 23(5): 3873-916.
34. Ali MH, Azad MAK, Khan KA, Rahman MO, Chakma U, Kumer A. Analysis of crystallographic structures and properties of silver nanoparticles synthesized using PKL extract and nanoscale characterization techniques. ACS Omega. 2023; 8(31): 28133-42.
35. Mehta K, Baruah PK. A comprehensive review and outlook on the experimental techniques to investigate the complex dynamics of pulsed laser ablation in liquid for nanoparticle synthesis. Rev Sci Instrum. 2022; 93(9): 091501. doi: 10.1063/5.0084803.
36. Hammed V, Bankole AA, Akinrotimi O, Ayanleye O. Silver nanoparticles (AGNPs): A review on properties and behavior of silver at the nanoscale level. Int J Sci Res Arch. 2024; 12(2): 1267-72.
37. Klinavicius T, Khinevich N, Tamuleviciene A, Vidal L, Tamulevicius

S, Tamulevicius T. Deep learning methods for colloidal silver nanoparticle concentration and size distribution determination from UV–vis extinction spectra. J Phys Chem C. 2024; 128(23): 9662-75.

38. Gogoi P, Deb S. Silver nanoparticles decorated wide band gap MoS2 nanosheet: enhanced optical and electrical properties. Plasmonics. 2025; 20(1): 575-83.
39. Luceri A, Francese R, Lembo D, Ferraris M, Balagna C. Silver nanoparticles: Review of antiviral properties, mechanism of action and applications. Microorganisms. 2023; 11(3): 629. doi: 10.3390/microorganisms11030629.
40. Awashra M, Młynarz P. The toxicity of nanoparticles and their interaction with cells: An in vitro metabolomic perspective. Nanoscale Adv. 2023; 5(10): 2674-723.